Operando atomic structure and active sites of TiO2(110)-supported gold nanoparticles during carbon monoxide oxidation

Marie-Claire Saint-Lager, Issam Laoufi, Aude Bailly

DOI: 10.1039/c2fd20157g

Operando atomic structure and active sites of TiO_2(110)-supported gold nanoparticles during carbon monoxide oxidation

Marie-Claire Saint-Lager[*]*, Issam Laoufi and Aude Bailly*

Institut Néel, CNRS et Université Joseph Fourier, BP 166, F-38042 Grenoble cedex 9, France

Abstract

It is well known that gold nanoparticles supported on TiO_2 act as catalyst for the CO oxidation, even below room temperature. Despite extensive studies, the origin of this catalytic activity remains debated. Indeed, when the particle size decreases, many changes may occur; thus modifying the nanoparticles' electronic properties and consequently their catalytic performances. Thanks to a state-of-the-art home-developed setup, model catalysts can be prepared in ultra-high vacuum and their morphology are then studied in *operando* conditions by Grazing Incidence Small Angle X-ray Scattering, as well as their atomic structure by Grazing Incidence X-ray Diffraction as a function of their catalytic activity. We previously reported on the existence of a catalytic activity maximum observed for three-dimensional gold nanoparticles with a diameter of 2-3 nm and a height of 6-7 atomic planes. In the present work we correlate this size dependence of the catalytic activity to the nanoparticles' atomic structure. We show that even when their size decreases below the optimum diameter, the gold nanoparticles keep the face-centered cubic structure characteristic of bulk gold. Nevertheless, for these smallest nanoparticles, the lattice parameter presents anisotropic strains with a larger contraction in the direction perpendicular to the surface. Moreover a careful analysis of the atomic-scale morphology around the catalytic activity maximum tends to evidence the role of sites with a specific geometry at the interface between the nanoparticles and the substrate. This argues for models where atoms at the interface periphery act as catalytically active sites for the carbon monoxide oxidation.

Introduction

It is now well established that gold nanoparticles (GNPs) supported on rutile TiO_2 act as catalysts for the oxidation of carbon monoxide (CO), even below room temperature.[1] Despite extensive studies, the origin and the mechanisms of the catalytic activity remain unclear. Most of the questions were focused on the activation of the oxygen molecule since there is experimental evidence that the limiting step of the reaction is the oxygen dissociation.[2] Depending on the kind of active sites, as well as the substrate type, several mechanisms were proposed. Some models assume that the reaction fully takes place on the GNPs surface where oxygen adsorption and dissociation can occur. In

[*] Corresponding authors : marie-claire.saint-lager@grenoble.cnrs.fr

that case the active sites are mainly identified as low-coordinated gold atoms.[3] The GNPs catalytic activity can also be due to quantum size effect linked to a metal-non metal transition appearing for clusters with thickness smaller than 1 nm.[4] Haruta *et al*. first suggested that the reaction could take place at the interfacial perimeter between the GNPs and the substrate.[5] This assumption was recently supported by studies that stress the crucial role of this perimeter in the CO oxidation, but the reaction mechanism is still strongly debated.

Kotobuki *et al*. demonstrated with temporal analysis of reactive products that active oxygen species can be stored on Au/TiO_2 catalysts at 350 K by exposure to thermal O_2 pulses.[6] They showed that the oxygen storage capacity and the CO oxidation activity of these catalysts scale with the perimeter length of the interface between the TiO_2 support and the GNPs. In the continuity of this work, Widmann *et al.* proposed a mechanism where CO adsorbed on the GNPs reacts with activated surface lattice oxygen species at the perimeter of the $Au\text{-}TiO_2$ interface.[7] At room temperature only the perimeter sites are involved whereas at higher temperatures (> 350 K), these oxygen species can be provided by migration on TiO_2 *via* oxygen vacancies. The authors concluded that those highly stable active oxygen species allow the facile dissociation of the oxygen molecule without assistance of any intermediate complex.

By means of a combination of infrared kinetic spectroscopic measurements and Density Functional Theory (DFT) calculations, Green *et al.* evidences that dual Ti-Au catalytic sites located at the perimeter interface of 3-nm GNPs supported on TiO_2 play a key role in the CO oxidation.[8] They indicate that O-O bond scission is activated by the formation of a $CO\text{-}O_2$ complex at these dual sites. They also stress the possibility for CO to adsorb either on Au or on TiO_2 sites thus giving two different sources of CO for the oxidation reaction, whereas the oxygen activation takes place around the perimeter area. These experiments carried out at low temperature (about 110 K) make it possible to distinguish which CO adsorption sites will first deliver the CO for the reaction indicating that the TiO_2 sites are energetically more favorable at such a low temperature. The CO adsorbed on top of the GNPs will only be able to diffuse to the active perimeter area at higher temperatures.

Fujitani *et al.* also stressed the importance of the nanoparticle-support periphery.[9] But according to the fact that CO oxidation on supported GNPs is greatly influenced by moisture, they suggest that reaction intermediates are rather OH- species.

A lot of attention was also dedicated to visualize GNPs at the atomic scale in real space and under reactive conditions. Yoshida *et al*. showed that the adsorption of carbon monoxide at room temperature induces the reconstruction of {100} facets of GNPs supported on CeO_2 during the CO oxidation.[10] The aberration-corrected environmental Transmission Electron Microscopy (TEM) images evidence that the carbon monoxide is preferentially adsorbed on the on-top sites of the gold atoms; the outermost gold layer forming an undulating hexagonal lattice. This reconstruction is observed for total pressures as high as 2.10^3 Pa. Although CO was thought to preferentially adsorb on the low-coordination sites, such as steps, edges and corners, this study evidences that atomically clean reconstructed {100} facets of roughly 4 nm-diameter GNPs are also able to adsorb it.

This illustrates that gaseous environments can strongly modified the GNPs atomic structure at the nanoscale. But deep structural changes can occur even in Ultra-High Vacuum (UHV) thus modifying the nanoparticles' electronic properties and consequently their catalytic properties. By means of aberration-corrected TEM, Walsh *et al.* studied carbon-supported gold nanoparticles in the size range for which they are usually known to be catalytically active, *i.e.* 2 to 10 nm. In UHV the multiply twinned icosahedral and decahedral structures turn out to be the most stable ones.[11] These highly strained GNPs (especially at the surface) are expected to be much more active than the single crystalline ones. Indeed, based on powder X-ray diffraction, Cunningham *et al.* found that, for $Au/Mg(OH)_2$, only catalysts with size distributions below 1 nm were active for CO oxidation. They identified two structural forms (cubo-octahedral and icosahedral) and observed that only the icosahedral one is catalytically active.[12] However such strained structure with a great number of low-coordinated atoms at the surface does not seem to be stable under annealing or even under the

microscope electron beam inducing sintering with the appearance of atomically clean surface facets in order to minimize the surface energy.[13] Anyway a lattice contraction is generally observed in very small particles. A decrease of the Au–Au distance with decreasing GNP size below a few nanometers was measured by Extended X-ray Absorption Fine Structure (EXAFS). According to the authors this effect could be responsible for the catalytic properties of the gold nanoparticles.[14]

This brief overview attests that all the recent developments allowing the observation of the structure at the atomic scale in reactive conditions pave the way toward a thorough understanding of the catalytic properties of supported GNPs. The present work comes within this scope. Thanks to a state-of-the-art home-developed setup, model catalysts can be prepared in UHV and their morphology then studied in *operando* conditions by Grazing Incidence Small Angle X-ray Scattering (GISAXS), as well as their atomic structure by Grazing Incidence X-ray Diffraction (GIXRD) as a function of their catalytic activity.[15,16] It was used to characterize gold nanoparticles supported on TiO_2(110) during CO oxidation, by recording at the same time the catalytic activity, GISAXS patterns and GIXRD data. We previously reported that the reaction rate dependence on the GNPs diameter presents a maximum for diameters of about 2 nm.[17,18] Above the maximum, the reaction rate well fits a power law of the diameter,[20] that is consistent with low-coordinated active sites located at the GNP interface periphery. However, this cannot explain the activity fall observed for GNPs smaller than 2 nm. The analysis of the evolution of the GNPs' atomic-scale structure and morphology around this maximum should yield a better understanding of the key parameters involved in their catalytic properties. Moreover, in contrast to atomic structures determined by X-ray measurements performed on powders, the use of nanoparticles epitaxially grown on a TiO_2(110) single crystal allows to get information on their shape, their atomic structure and their lattice parameter parallel and perpendicular to the substrate surface. In this frame, GISAXS and GIXRD lead to define what can be called an 'average' particle analyzed in the reciprocal space and representing a wide collection of nanoparticles. In that sense it is a good complement of local probes such as TEM or Scanning Tunneling Microscopy (STM). Moreover these X-ray techniques can easily be operated in *operando* conditions, the simultaneous determination of the reaction rate allowing a direct correlation with the geometrical parameters of the average GNP.

Experimental method

The experiments were performed in a home-developed setup consisting of an UHV preparation chamber connected to a batch reactor running from UHV up to reactive conditions at ambient pressures and allowing both X-ray scattering and catalytic activity measurements in static conditions.[18,19] The setup is operated on the "2+2" diffractometer of the GMT station at the beamline BM32 of the European Synchrotron Radiation Facility (ESRF).[17] The experimental procedure was previously detailed;[19,20] we summarize the main features hereafter. The GNPs were synthesized in the UHV preparation chamber (base pressure of 5.10^{-8} Pa). The TiO_2(110) single crystal, used as a substrate, was first bombarded with 750 eV argon ions and then annealed at 1000 K under an oxygen partial pressure of 10^{-3} Pa in order to restore the surface stoichiometry.[19] Gold nanoparticles were grown by UHV vapor deposition at 300 K from a Knudsen cell. As calibrated by a quartz microbalance, the average thickness of the gold deposit was ranging between 0.05 and 3 atomic monolayers (1 ML corresponding to 0.235 nm, equivalent to one Au(111) atomic layer). Once prepared, the Au/TiO_2 (110) samples were transferred under UHV into the batch reactor in order to perform X-ray and catalytic activity measurements during the carbon monoxide oxidation. The measurement procedure involved three steps; each lasting approximately two to three hours: (1) Au/TiO_2(110) was first studied in UHV (2.10^{-7} Pa) at room temperature (RT), (2) then during annealing at 473 K in 2.10^{3} Pa of oxygen, (3) and finally during CO conversion into CO_2 that started by adding 20 Pa of CO to the oxygen, while keeping the sample at 473 K. The CO and CO_2 partial pressures in the reactor were deduced respectively from the 28 and 44 ionization currents measured by a mass spectrometer. The gas composition was followed as soon as the sample was introduced in the

batch reactor and all along the experimental procedure. During the step (3), the reaction rate was defined as the number of CO molecules converted into CO_2 per gold atom per second on the basis of the total number of gold atoms.[19] The GISAXS patterns were generally acquired at the beginning and at the end of each step. In between, diffraction spectra were collected along several directions in the reciprocal space.

To enhance the GNPs' signal, X-ray measurements were performed with a photon energy of 18 keV at a grazing incidence close to the critical angle (0.13° for TiO_2 at 18 keV). A shutter, opened only during X-ray data collection, was mounted in order to avoid long time exposures to the X-ray beam and consecutive sample surface damages. Finally, no significant difference could be observed in either the scattering or the catalytic activity with and without photons on the sample. For GIXRD measurements, a standard NaI scintillator detector was used and the GISAXS patterns were collected on a 2D camera (Princeton Instruments, pixel size of 56.25 μm).[18]

The structure of bulk gold is face centered cubic (fcc) and two kinds of epitaxy relationships are usually observed on $TiO_2(110)$: $(112)_{Au}//(110)_{TiO2}$ and $(111)_{Au}//(110)_{TiO2}$, depending on the substrate temperature during the GNPs growth.[20] However, by means of GIXRD in UHV, Lazzari *et al.* found that these two epitaxial relationships are nearly equiproportional whatever the temperature.[21] For the two epitaxy orientations gold grows with the $<110>_{Au}$ direction of the dense rows aligned with the $<001>_{TiO2}$ of the oxygen ones, the interatomic distances being 0.296 nm for TiO_2 and 0.2886 nm for gold. As usual in surface crystallography, the *z* direction is perpendicular to the surface, that means along the $<110>_{TiO2}$ direction, and the *x* direction has the smallest lattice parameter that is along $<001>_{TiO2}$. The unit cell parameters are thus equal to $a = 0.296$ nm, $b = c = 0.6492$ nm. The present diffraction measurements show that the $(111)_{Au}//(110)_{TiO2}$ epitaxy is predominant, especially under reactive conditions. For convenience the gold lattice is described in its hexagonal cell. The schematic representation of the fcc gold reciprocal space (with Miller indices: H_{Au}, K_{Au}, L_{Au}) over the $TiO_2(110)$ one (with Miller indices: H_{TiO2}, K_{TiO2}, L_{TiO2}) is given in Fig. 1a for $L = 0$. Fig. 1b is a 3D schematic representation of the gold reciprocal space for the two kinds of stacking usually observed along the <111> trigonal axis.

For each gold deposit, the mean geometrical parameters of the GNPs, such as the diameter D, the height H and the interparticle distance L, were deduced from the quantitative analysis of the GISAXS patterns performed using the IsGISAXS software.[22] These measurements are detailed elsewhere.[18,19,20] Considering the whole set of samples measured *in operando*, the best fit of the GISAXS patterns was obtained assuming a truncated sphere to model the GNPs shape. The geometrical parameters are an average value of those obtained for the two main $TiO_2(110)$ surface directions. In contrast to the interparticle distance L, the diameter D was found identical in these two directions with decreasing value when the deposited equivalent gold thickness diminishes. Fig. 2 sums up the main results concerning the dependence of the CO conversion rate as a function of the mean geometrical parameters deduced from the quantitative analysis of the GISAXS patterns recorded in real time.[19]

Results

Evolution of the diffraction spectra under reactive gases

The evolution of the diffraction spectra obtained during the three steps of the experimental procedure is illustrated in Fig. 3 for a sample with an equivalent gold thickness of 0.1 ML (Fig. 3a and 3c) and another one with 0.5 ML (Fig. 3b and 3d). Two directions of the reciprocal space are represented: parallel to the surface along H and perpendicularly to it along the rod $(0\ 1)_{Au}$.

For the H-scan, the Au (2 -1 0)$_{Au}$ Bragg peak is expected at $H_{TiO2} = 2.05$ (Fig. 3a and 3b). In UHV, its position is found at a higher value, and the shift is larger when the gold thickness decreases (corresponding to smaller particles). For 0.1 ML, the quantitative GISAXS analysis gave 1 nm for the diameter and 0.6 nm for the height and the Au (2 -1 0)$_{Au}$ peak was found at $H_{TiO2} = 2.11 \pm 0.02$. It corresponds to a lattice contraction of 3.4 %. In the case of the 0.5 ML deposit, the nanoparticles are larger; the diameter being 2.2 nm and the height 1.5 nm. The gold maximum is found at $H_{TiO2} = 2.07 \pm 0.01$ indicating that there is still a small lattice contraction of 0.8 %. When annealing at 473 K and also after introducing CO for starting the oxidation reaction, strong changes are observed for the thinnest deposit, whereas at 0.5 ML there is only a gentle evolution. Above 1 ML, the spectra remained independent of the environment. This behavior can be correlated to what was deduced from GISAXS patterns measured at the same time.

Under reaction conditions (step 3), for the 0.1 ML sample, the diameter grows up to 1.7 nm and the height to 1.2 nm, as deduced from GISAXS, and the gold peak shifts to $H_{TiO2} = 2.06 \pm 0.02$, a value closer to the bulk gold one. For the 0.5 ML deposit, the peak reaches the position of the bulk value. In that case, we can observe that there is a subtle difference between step (2) and step (3); the relaxation seeming slightly larger under oxygen than under reactive conditions.

Along the (0 1)$_{Au}$ rod and during the step (1), in UHV and at room temperature, the intensity collected for 0.1 ML, with a height of about 3 atomic planes, presents only one main broad peak (Fig. 3c). For the 0.5 ML, the height corresponds to at least 6 atomic planes and in that case, the diffraction spectra exhibit well defined peaks at $L_{Au} = 1, 2, 4, 5$ (Fig. 3d) characteristic of the two sequences ABC and ACB of the fcc stacking. In the case of the 0.1 ML deposit, the fcc ordering is progressively induced by gas adsorption at 473 K. Indeed, under oxygen at 473 K (step 2), the main broad peak starts to split into two peaks. Then, under reaction conditions at 473 K, the nanoparticles height increases up to 6 atomic planes. In the same conditions, the peaks of the 0.5 ML deposit only slightly increase and become a little bit thinner.

Au-Au distances and catalytic activity

The interatomic distances d_{Au-Au} in the gold nanoparticles during reaction were deduced from the diffraction spectra. Perpendicularly to the surface, it was obtained by averaging the position of the peak at $L = 2$ and 4 along the (0 1)$_{Au}$ rod with the one for $L = 3$ of the (2 -1)$_{Au}$ rod. This choice allowed cancelling the shift of the peaks due to defects in the fcc stacking. In the surface plane, it was calculated by deconvoluting the gold peaks from the TiO_2 one in the radial scan around (200)$_{TiO2}$. Besides, we verified that the width of the gold peaks is consistent with the size deduced by GISAXS. The variation of the Au-Au distances is reported in Fig. 4 as a function of the particles diameter. They were normalized to the bulk gold values that are $d_{\perp} = a_0/\sqrt{3}$ and $d_{//} = a_0/\sqrt{2}$; the bulk Au cubic lattice parameter a_0 being 0.408 nm. A contraction is observed for sizes below$\approx$ 2-3 nm, as already reported by using EXAFS.[16] But in the present case, the Fig. 4 shows that this effect is clearly anisotropic: it is almost negligible in the surface plane whereas it is quite significant perpendicularly to it. This can be correlated to the shape of the nanoparticles, since the aspect ratio H/D is less than 1 and decreases in this region from 0.7 to 0.5. Interestingly, the comparison with the variation of the catalytic activity for CO oxidation in Fig.4 indicates that this contraction coincides with the fall of the catalytic activity below the optimum diameter.

Geometry of the active sites

Looking at the geometrical parameters of the nanoparticles corresponding to the drop of the activity below the optimum diameter, we observed that the slope of the variation of the mean height H as a function of the diameter becomes more abrupt (Fig. 2). This means that nanoparticles become flatter in this particular region. Actually, in the region around the maximum of activity, the value of the mean diameter varies slowly while the height changes more significantly. It is thus interesting to plot the variation of the GNP geometrical parameters as a function of the particles height and to

correlate it to that of the activity for CO oxidation such as in Fig. 5. It shows that the diameter is more or less constant in the region of the maximum of activity indicating that it is not the essential parameter. At first sight, the models, where the reaction occurs at the interface perimeter between the GNPs and the TiO_2 surface, would expect that the variation of the CO conversion rate per Au atom would follow the same variation as the fraction of Au atoms on the perimeter.[11] Fig. 5 shows that it is not the case here since this fraction continuously increases when the particles size decreases, including while crossing the maximum of activity. In contrast, the aspect ratio H/D presents a behavior similar to the activity with a maximum for the same value of the height indicating that the geometry of the particles at the interface is a crucial parameter. The schemes inserted in fig. 5 evidence that the maximum of activity corresponds to a sharp angle θ between the GNP surface tangent and the substrate. The fall on both sides of the maximum corresponds to θ becoming closer to a right angle. This suggests that the active sites could result from the combined action of several atoms near the perimeter. Thereby, a kind of cavity is created where low-coordinated Au atoms and the titania substrate can interact simultaneously with the reaction entities.

To get more informations we need to use an atomic model to describe the GNPs structure. Most of the images obtained by TEM with atomic resolution evidenced a shape close to cubo-octahedrons for particles size in the range of the present work and moreover with a (111) face in contact with the substrate surface.[23,24,25] Consistently, as shown hereabove, the diffraction data collected for sample under reactions conditions reveal a fcc structure with the <111> direction perpendicular to the surface that is compatible with such cubo-octahedrons.[26] However, we did not find any trace of signal indicating well-defined facets on the recorded GISAXS patterns, which would present oriented rods corresponding to the (111) and (100) planes as observed for well-ordered facetted supported clusters.[27] This may be due to a misorientation of the gold nanoparticles or to particles too small to present facets large enough to be seen by GISAXS. Therefore the truncated sphere used to model the nanoparticles for quantitative analysis of the GISAXS patterns is a quite good approximation. The two parameters needed to define the corresponding truncated cubo-octaedrons are *m* and *l,* the number of atoms on the edges and the number of atomic planes parallel to the surface, respectively. Their relationships with the diameter D and the height H measured by GISAXS were established in ref . 20 in line with reference:[28]

$$3m - 2 \cong N_D = (D - 2r_{Au})/(d_{//} + 1)$$

and $$l = (H - 2r_{Au})/(d_{\perp} + 1),$$

N_D being the number of atoms along the diameter D and $r_{Au} = 0.026$ nm, the gold atomic radius as seen by X-rays. The variation of the interatomic distance $d_{Au\text{-}Au}$ mentioned above is neglected here and the bulk values for $d_{\perp}$ and $d_{//}$ are used.

As shown in Fig. 6, the experimental data do not exactly match with integer values of *m* and *l*. They represent the center of the size distribution of the GNPs on the TiO_2 substrate. The width of this distribution in the two directions is represented by error bars in the insert of Fig. 6. For the height, it can be interpreted as a distribution of particles with different number of atomic layers; it varies noticeably as a function of the particle size. For the flattest nanoparticles, the error bar is large and due to a wide distribution of the size on the sample. For the biggest ones, the truncated sphere becomes a less good approximation of the GNPs shape that begins to present well defined facets, enlarging the value of the error. In the middle range, that means close to the optimum size for the activity, the particles height has a thin distribution ($l = 7 \pm 0.5$ at the maximum). As previously reported this is a consequence of the sintering induced by the temperature and then by the reaction itself.[19,20] Concerning the dispersion width of the diameter, it is roughly constant and corresponds to ± 2 atoms. Thus, it cannot be attributed to a distribution of octahedrons with several *m* integers. Indeed, a distribution with *m* and *m* + 1 atoms on the edge would correspond to diameter with N_D and $N_D + 3$ respectively and would thus result in a bimodal distribution for the diameter, that is definitively not observed. This indicates that GNPs shape is not ideal. For instance, a twin structure was evidenced for nanoparticles exposed to 1 vol % CO in air (100 Pa) by High Resolution TEM (HRTEM).[SOM27]

However, we can observe that all the experimental data are localized close to an integer value of *m* (less than ±1 atom), that means with a shape not far from the ideal cubo-octahedron model.

Fig.6 shows that the data below the optimum have *m* close to 3, when the number of layers *l* grows, the reaction rate increases (vertical red arrow in Fig. 6). Above the optimum size for the (almost) same number of layers, the activity increases when *m* goes down to 3 (horizontal red arrow in Fig. 6). For higher values of *m*, the main factor prevailing for the activity fall is the rapid decrease of the fraction of potentially active sites at the surface relatively to the total number of atoms in the particles. Finally, the maximum of activity occurs for particles close to cubo-octahedron with $m = 3$. The main feature of this GNPs morphology is the presence of edges parallel and close to the substrate surface. They connect a (111) hexagonal face of the upper part of the particles and a (100) square face that makes a sharp angle of 55° with the TiO_2 surface. The combination of such an angle, together with low-coordinated gold atoms on the edges in the vicinity of the substrate surface constitute a particular geometry that could be very active sites for the CO oxidation.

Conclusion

In this work we studied the structural properties and the morphology of the GNPs around the maximum observed for the CO oxidation reaction rate as a function of the particles diameter, thanks to *in operando* GISAXS, GIXRD and activity measurements. For GNPs bigger than 2-3 nm, that is above the optimum size for the catalytic activity, the fcc structure is already established during the gold growth on $TiO_2(110)$. For the smallest ones, the fcc ordering appears only after annealing at 473K and under reactive gas pressure. Before adding 20 Pa of CO, starting the oxidation reaction, the GNPs were exposed to 2.10^3 Pa of oxygen at 473K. The diffraction data present a subtle difference between the two steps with the relaxation of the Au-Au distance that seems slightly larger under oxygen than under reactive conditions. This may be due to oxygen interaction with outermost atoms of the GNPs which could provoke a dilatation of the Au-Au distances (the measured value is an average over the particle). As already reported, under oxygen pressure, gold is probably pre-oxidized, thus producing $Au^{\delta+}$ sites on the GNP surface.[29] Such positively charged Au site was also evidenced under high pressure of oxygen at room temperature by X-ray Photoelectron Spectroscopy (XPS),[30,31] as well as by X-ray Absorption Near-Edge Structure (XANES).[32] This gold activation was attributed to X-rays.[33] Such a pre-oxidation step was shown to modify the reaction pathway at low temperature (120K), since it deactivates the most reactive sites.[31] However, in most of the cases, CO introduction quickly reduced gold to its metallic form,[33,34] all the more since the temperature is equal to 473K in the present study. The interaction of oxygen with GNPs was also observed by HRTEM leading to rounded GNPs.[33] In a more recent work, Uchiyama *et al.* drew the diagram of the GNPs morphology grown on CeO_2 as a function of the O_2 and CO partial pressures.[26] According to it, the pressure conditions of step (2) of the present study correspond to the domain where the GNPs are rounded. In reaction conditions (*i.e.* after CO introduction) the diagram indicates that the GNPs should be well facetted.

Under reaction conditions, the GNPs have the fcc bulk structure with the $<111>_{Au}$ direction perpendicular to the $TiO_2(110)$ surface. However, for diameters below 2-3 nm, they are anisotropically strained with a contraction perpendicularly to the surface that can reach 2% whereas it is negligible in the parallel direction. This contraction of d_{Au-Au} coincides with the fall in the catalytic activity below the optimum size. A deeper structural analysis is in progress to determine if more significant structural changes occur in this size range to explain the fall of the GNPs catalytic activity.

In the present work, we show that the maximum of activity corresponds to a sharp angle between the GNP surface tangent and the substrate. This work confirms the dominating role of the sites at the interface but with a specific geometry involving substrate atoms and several atoms of the GNPs. The temperature being 473 K, the diffusion on the GNPs surface as well as on the TiO_2 surface cannot be the limiting factor as for studies done at much lower temperatures (around 100 K).[9,31] This

would claim for models involving the existence of intermediate complexes on mixed adsorption sites to activate the oxygen molecules.

These results on TiO_2(110)-supported GNPs show that the combination of GISAXS, GIXRD and catalytic activity measurements is a very promising way to examine at the atomic scale nanoparticles with sizes around 2 nm and below while they are catalyzing a given reaction.

Acknowledgements

The technical staffs (SERAS and MCMF) of Institut Neel-CNRS and of the BM32 CRG beamline at ESRF are acknowledged for their assistance. We also thank Rémi Lazzari and Jacques Jupille of the INSP for their help during the synchrotron experiments."

1 M. Haruta, N. Yamada, T. Kobayashi and S. Iijima, *J. Catal.*, 1989, **115**, 301.
2 V. A. Bondzie, S. C. Parker and C. T. Campbell, *Catal. Lett.*, 1999, **63**, 143.
3 M. Mavrikakis, P. Stoltze and J.K. Nørskov, *Catal. Lett*., 2000, **64**, 101.
4 M. Valden, X. Lai and D.W. Goodman, *Science*, 1998, **281**, 1647.
5 M. Haruta, S. Tsubota, T. Kobayashi, H. Kageyama, M. J. Genet and B. Delmon, *J. Catal.,* 1993, **144,** 175; M. Haruta, *Catal. Today,* 1997*,* **36**, 153; M. Haruta, *Faraday Disc.* 2011, **152**, 1
6 M. Kotobuki, R. Leppelt, D.A. Hansgen, D. Widmann and R. J. Behm, *J. Catal*., 2009, **264**, 67.
7 D. Widmann and R. J. Behm, *Angew. Chem. Int. Ed.*, 2011, **50**, 10241.
8 I. X. Green, W. Tang, M. McEntee, M. Neurock and J. T. Yates, Jr., *Science* **333** (2011) 736
9 T. Fujitani and I. Nakamura, *Angew. Chem. Int. Ed*., 2011, **50**, 10144
10 H. Yoshida, Y. Kuwauchi, J. R. Jinschek, K. Sun, S. Tanaka, M. Kohyama, S. Shimada, M. Haruta and S. Takeda, *Science,* 2012, **335**, 317.
11 M. J. Walsh, K. Yoshida, A. Kuwabara, M. L. Pay, P. L. Gai and E. D. Boyes, *Nano Lett*., 2012, **12**, 2027.
12 D. A. H. Cunningham, W. Vogel, H. Kageyama, S. Tsubota, and M. Haruta, *J. Catal.,* 1998, **177**, 1.
13 M. J. Walsh, K. Yoshida, M. L. Pay, P. L. Gai and E. D. Boyes, *ChemCatChem*, 2012, **4**, 1638.
14 J. T. Miller A.J. Kropf, Y. Zha, J.R. Regalbuto, L. Delannoy, C. Louis, E. Bus and J.A. van Bokhoven, *J. Catal.*, 2006, **240**, 222.
15 M.-C. Saint-Lager, A. Bailly, P. Dolle, R. Baudoing-Savois, P. Taunier, S. Garaudée, S. Cuccaro, S. Douillet, O. Geaymond, G. Perroux, O. Tissot, J.-S. Micha, O. Ulrich and F. Rieutord, *Rev. Sci. Instrum.,* 2007, **78**, 083902.
16 M.-C. Saint-Lager, A. Bailly, M. Mantilla, S. Garaudée, R. Lazzari, P. Dolle, O. Robach, J. Jupille, I. Laoufi and P. Taunier, *Gold Bull.,* 2008, **41**, 159.
17 I. Laoufi, M.-C. Saint-Lager, R. Lazzari, J. Jupille, O. Robach, S. Garaudée, G. Cabailh, P. Dolle, H. Cruguel and A. Bailly, *J. Phys. Chem. C,* 2011, **115**, 4673.
18 M.-C. Saint-Lager, I. Laoufi, A. Bailly, O. Robach, S. Garaudée and P. Dolle, *Faraday Discuss.,* 2011, **152**, 253.
19 J.-M Pan, B. L. Maschhoff, U. Diebold and T. E. Madey, *J. Vac. Sci. Technol. A,* 1992, **10***,* 2470.
20 F. Cosandey, L. Zhang and T. E Madey, *Surf. Sci.,* 2001, **474**, 1.
21 R. Lazzari, G. Renaud, J. Jupille and F. Leroy, *Phys. Rev. B*, 2007, **76**, 125412.
22 R. Lazzari, *J. Appl. Crystallogr.,* 2002, **35,** 406, http://www.insp.upmc.fr/axe2/Oxydes/IsGISAXS/isgisaxs.htm
23 S. Giorgio, M. Cabié and C.R. Henry, *Gold Bull.*, 2008, **41**, 167.
24 T. Uchiyama, H. Yoshida, Y. Kuwauchi, S. Ichikawa, S. Shimada, M. Haruta, and S. Takeda, *Angew. Chem. Int. Ed,*. 2011, **50**, 10157.
25 Y. Kuwauchi, H. Yoshida, T. Akita, M. Haruta and S. Takeda*, Angew. Chem. Int. Ed.* 2012, **51**, 7729.
26 R. Van Hardeveld and F. Hartog, *Surf. Sci.*, 1969, **15**, 189.

27 M. Rauscher, R. Paniago, T.H. Metzger, Z. Kovats, J. Domke, H.D. Pfannes, J. Schulze and I.J. Eisele, *Appl. Phys.*, 1999, **86**, 6763.
28 A. Carlsson, A. Puig-Molina and T. V. W. Janssens, *J. Phys. Chem. B*, 2006, **110**, 5286.
29 I. X.Green, W. Tang, M. McEntee, M. Neurock and J. T. Yates, Jr , JACS, *J. Am. Chem. Soc*., 2012, **134**, 12717.
30 P. Jiang, S. Porsgaard, F. Borondics, M. Köber, A. Caballero, H. Bluhm, F. Besenbacher, M. Salmeron, *J. Am. Chem. Soc*., 2010, **132**, 2858.
31 K. Dumbuya, G. Cabailh, R. Lazzari, J. Jupille, L. Ringela, M. Pistor, O. Lytkena, H.-P. Steinrück, J.M. Gottfried, *Catal. Today*, 2012, **181**, 20.
32 J.A. van Bokhoven, C.Louis, J. T. Miller, M. Tromp, O. V. Safonova and P. Glatzel*, Angew. Chem. Int. Ed.*, 2006, **45,** 4651.
33 S. Giorgio, S. Sao Joao, S. Nitsche, D. Chaudanson, G. Sitja, C.R. Henry*, Ultramicroscopy*, 2006, **106**, 503.

Figures captions

Fig. 1: Schematic representations of the reciprocal space of $(111)_{Au}//(110)_{TiO2}$ **(a)** at L=0 with in black the TiO_2 peaks (filled circles: Bragg peaks and empty circles: cut of the surface rods) and in orange the gold Bragg peaks. H_{TiO2}, K_{TiO2} and L_{TiO2} are the Miller indices in the frame of the $TiO_2(110)$ surface. The hexagonal cell of the fcc bulk gold is represented in orange. **(b)** 3D representation of the gold reciprocal space. The orange spots represent the Bragg peaks of the ABC stacking and the blue ones those of the ACB one. The dark red spots are peaks common to the two stackings. In the two schemes the green arrows indicate the directions along which the diffracted intensity was collected for Fig. 3.

Fig. 2: Variation of the CO conversion reaction rate into CO_2 per Au atom per second (black) and of the mean height H (blue) as a function of the mean diameter D (blue) of the GNPs measured *in operando*. The full lines are guides for the eyes.

Fig. 3: Diffracted intensity: (a) and (b) along a radial scan around $(2\ -1\ 0)_{Au}$ and (c) and (d) along the $(01)_{Au}$ rod for two samples with gold equivalent thicknesses of : (a) and (c) 0.1 ML and (b) and (d) 0.5ML during the three steps of the experimental procedure. (1) in UHV at RT (black), (2) under 2.10^3 Pa of oxygen at 473 K (blue) and (3) after adding 20 Pa of CO while keeping T = 473 K (red). In (a) et (c) the thin peak centered at $(200)_{TiO2}$ with a broad and intense feet is the TiO_2 Bragg peak, the shoulder on the right is the $(2\ -1\ 0)_{Au}$ Bragg peak that is expected at $(2.05\ 0\ 0)_{TiO2}$ for bulk Au as indicated by the grey dashed line.

Fig. 4: Variation of the CO conversion reaction rate into CO_2 per Au atom per second (black) and of the interatomic distance $d_{Au\text{-}Au}$, normalized to the bulk gold value, (blue and red : perpendicular and parallel to the surface, respectively) as a function of the GNPs' mean diameter *D*. All the parameters were measured *in operando* during CO oxidation (step (3)): the catalytic activity by mass spectrometry, the diameter D was deduced from GISAXS and $d_{Au\text{-}Au}$ from the diffraction measurements. The full lines are guides for the eyes.

Fig. 5: Comparison of the variation of the GNPs geometrical parameters around the catalytic activity maximum as a function of the height. (black) Reaction rate of the CO conversion into CO_2 per Au atom per second, (blue) diameter D of the GNPs, (grey) ratio between N_P and N_V, the number of atoms at the interface perimeter between the nanoparticles and the TiO_2 substrate and the number of total number of atoms within the GNPs, respectively, and (red) the aspect ratio H/D. A schematic representation of the supported nanoparticles is given with, on the left, H/D = 0.5 and on the right, H/D = 0.7 as observed close to the catalytic activity maximum. θ is the angle between the GNP surface tangent and the substrate.

Fig. 6: Reaction rate of the GNPs as a function of the size of the corresponding truncated cubo-octahedron with, on the vertical axis the number of atomic layers *l*, and on the bottom horizontal axis, *m,* the number of atoms on the edges and on the upper one, N_D, the number of atoms along the diameter; the scales for *l*, N_D and *m* are proportional to the value of $d_\perp$, $d_{//}$ and $3d_{//}$, respectively. The red spots are proportional to the reaction rate for CO oxidation, as deduced from the experimental data. They are located at the *m* and *l* values deduced from the mean D and H, as explained in the text. Schematic representations of cubo-octahedrons are given for several couples of (*m,l*) pointed by the blue arrows (see text for the red arrows). The couples (*m*,*l*) corresponding to complete cubo-octahedron are marked by dark blue diamonds. On the lower grey dashed line, the aspect ratio *H/D* is 0.5 and it is 0.8 on the upper one, that crosses the dark blue diamonds. The part of the diagram above it has been shaded since the corresponding (*m*,*l*) couples cannot be assigned to the cubo-octahedral geometry. In the insert, the experimental data were also plotted as a function of *l* (vertical axis) and N_D (upper horizontal axis) with their error bars calculated from the width of the Gaussian distribution of the GNPs size given by the GISAXS analysis.

Figure 1

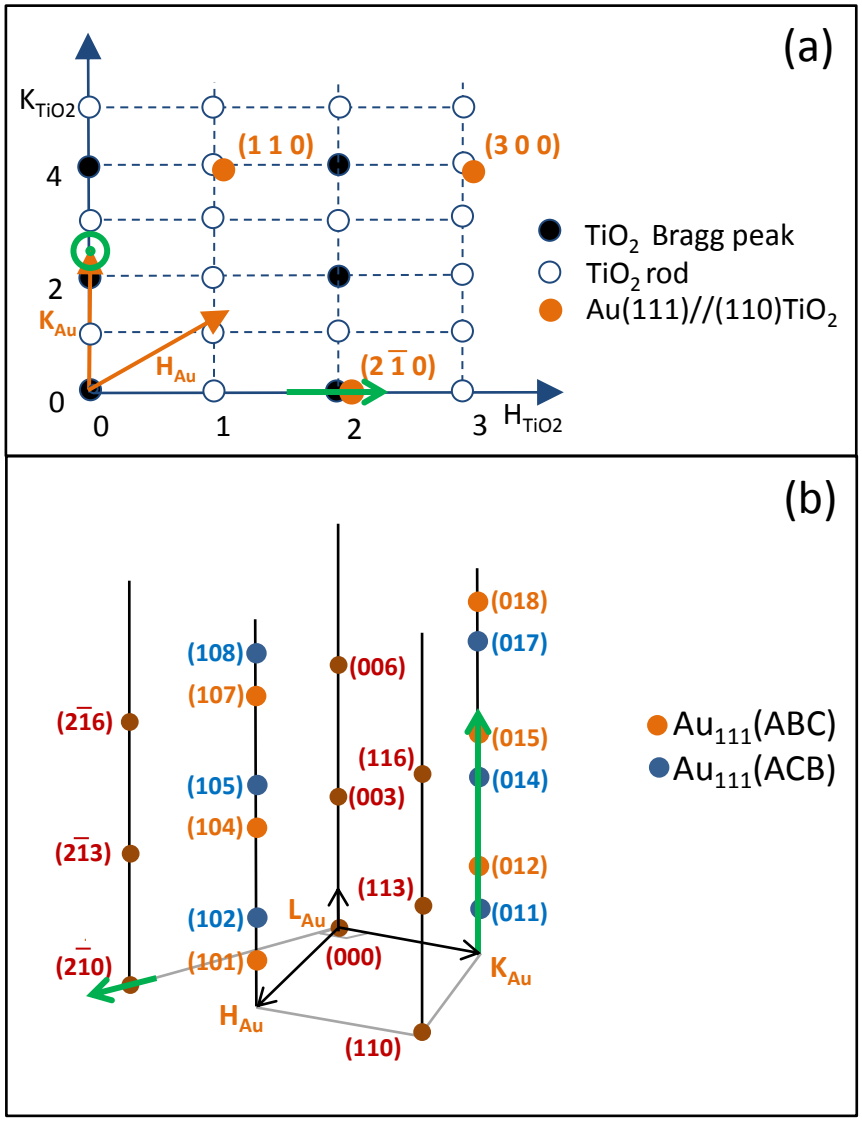
(a)
K_{TiO2}
4
2
0
K_{Au}
H_{Au}
(1 1 0)
(3 0 0)
(2 $\bar{1}$ 0)
0
1
2
3
H_{TiO2}
TiO_2 Bragg peak
TiO_2 rod
Au(111)//(110)TiO_2
(b)
(018)
(017)
(108)
(107)
(006)
(2$\bar{1}$6)
(015)
(116)
(105)
(014)
(003)
(104)
(2$\bar{1}$3)
(012)
(113)
L_{Au}
(102)
(011)
(2$\bar{1}$0)
(101)
(000)
K_{Au}
H_{Au}
(110)
Au_{111}(ABC)
Au_{111}(ACB)

Figure 2

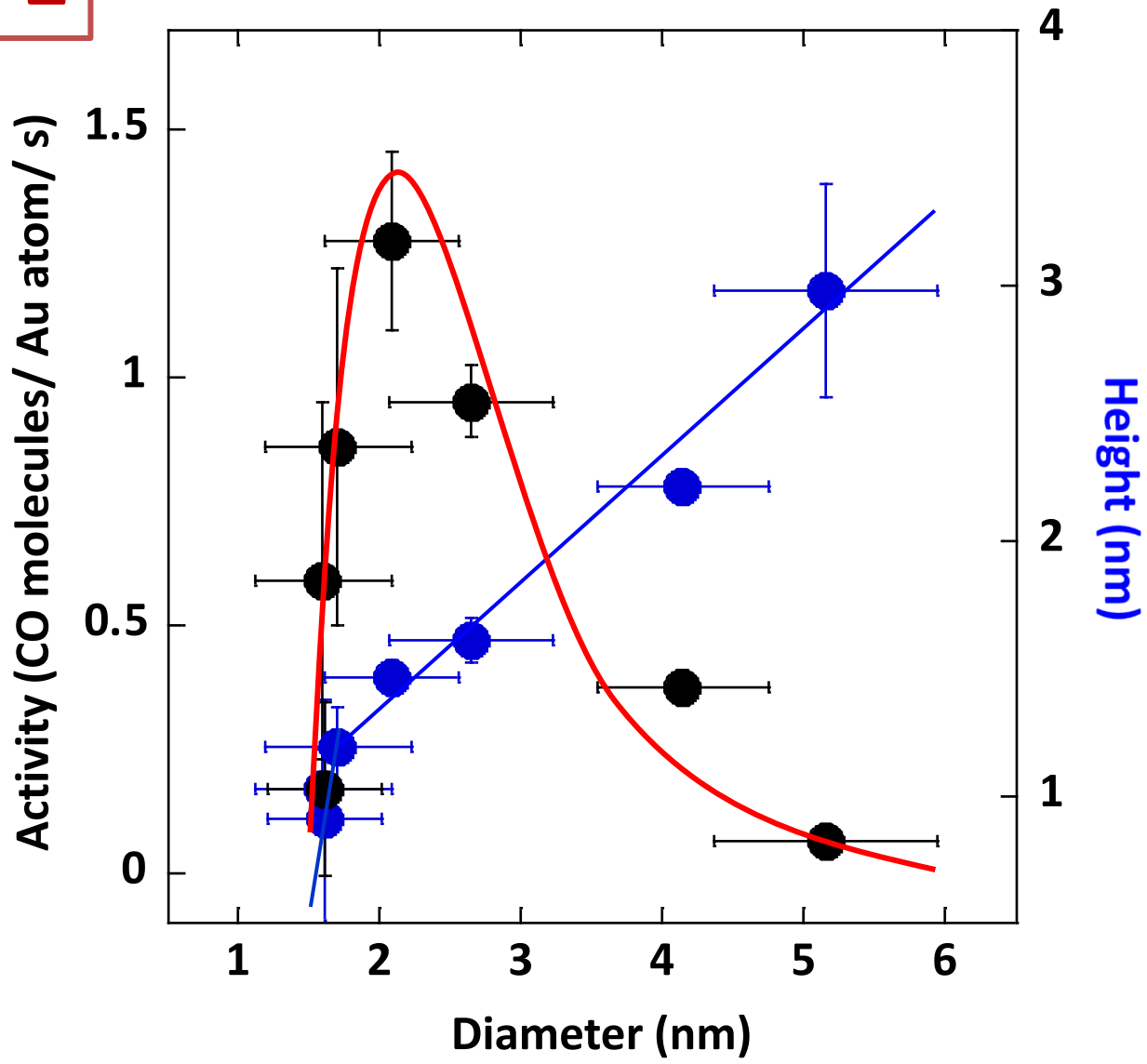
Activity (CO molecules/ Au atom/ s)
1.5
1
0.5
0
1
2
3
4
5
6
Diameter (nm)
4
3
2
1
Height (nm)

Figure 3

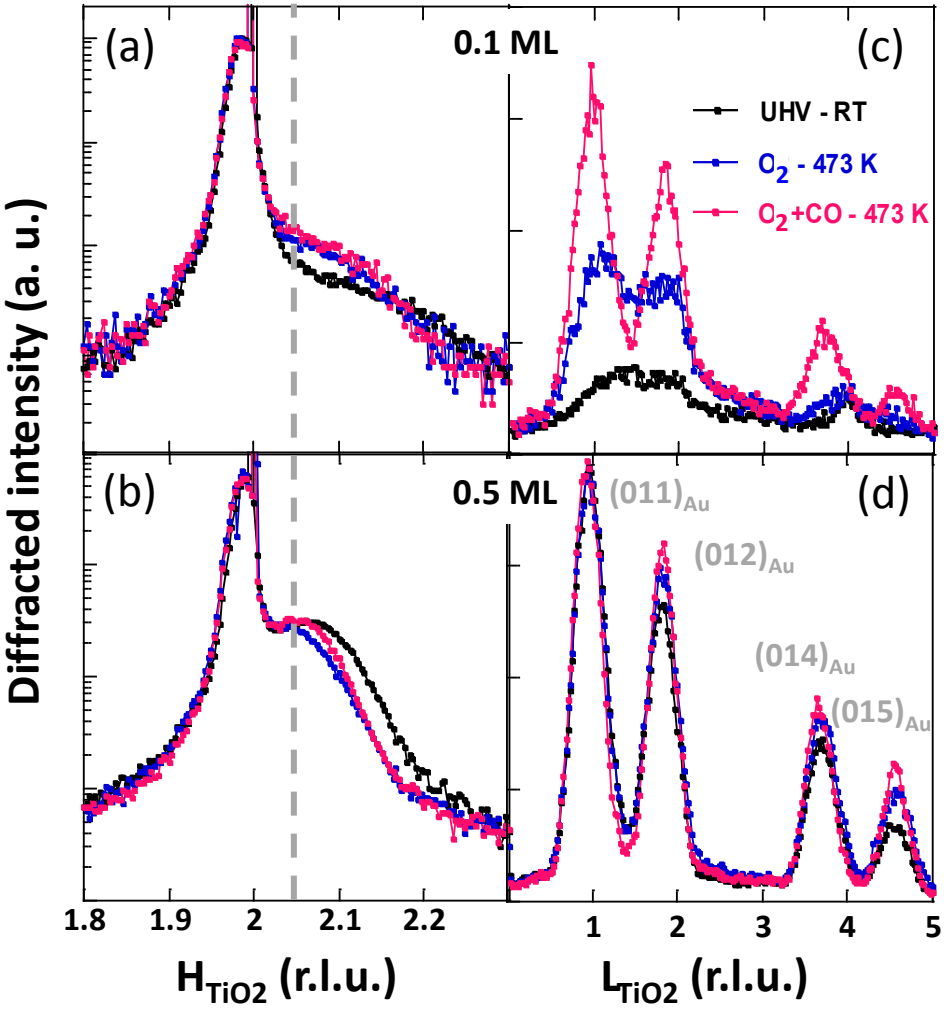
(a)
0.1 ML
(c)
UHV - RT
O2 - 473 K
O2+CO - 473 K
(b)
0.5 ML
(d)
(011)Au
(012)Au
(014)Au
(015)Au
Diffracted intensity (a. u.)
1.8
1.9
2
2.1
2.2
HTiO2 (r.l.u.)
1
2
3
4
5
LTiO2 (r.l.u.)

Figure 4

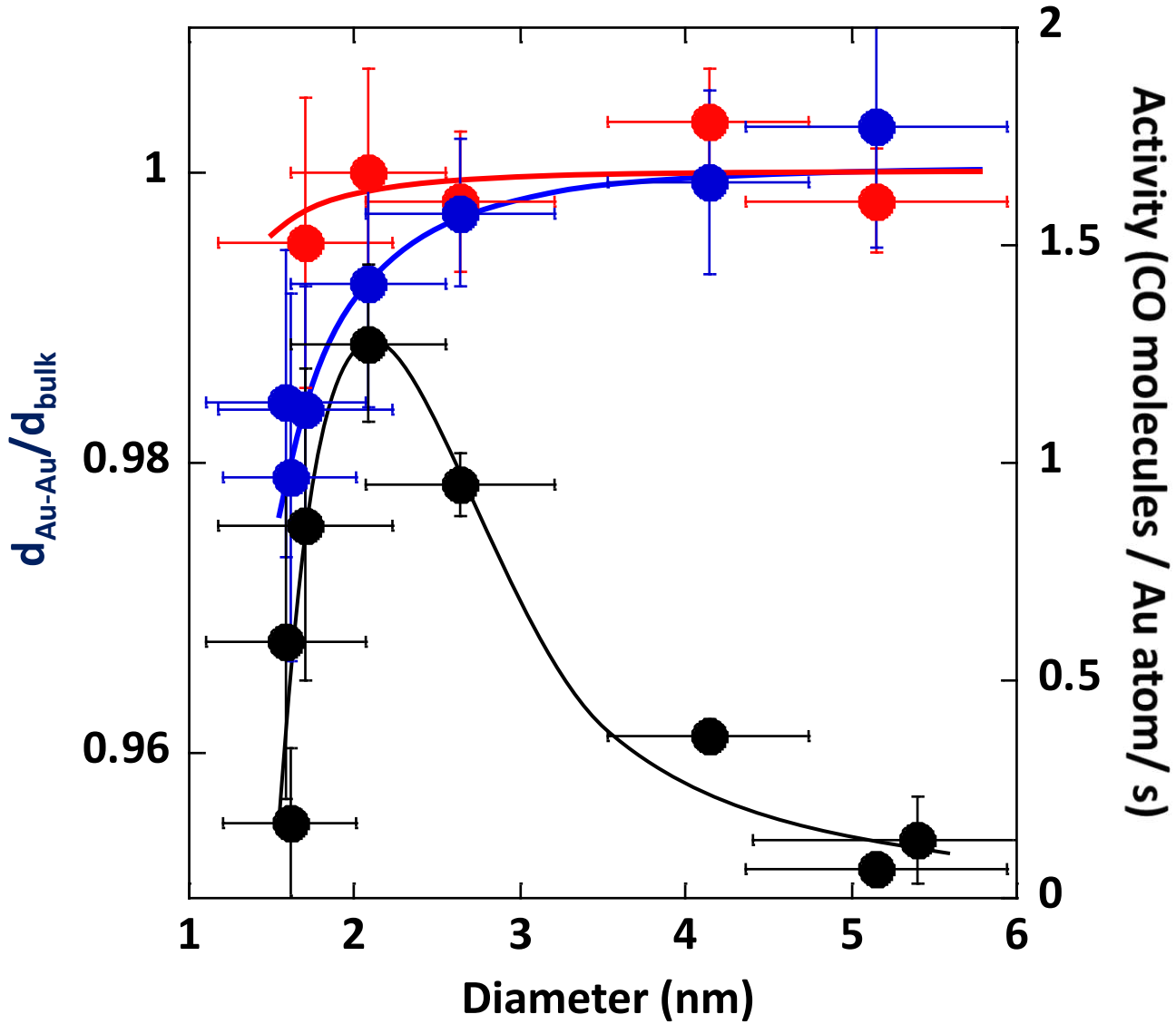
d_{Au-Au}/d_{bulk}
1
0.98
0.96
1
2
3
4
5
6
Diameter (nm)
2
1.5
1
0.5
0
Activity (CO molecules / Au atom/ s)

Figure 5

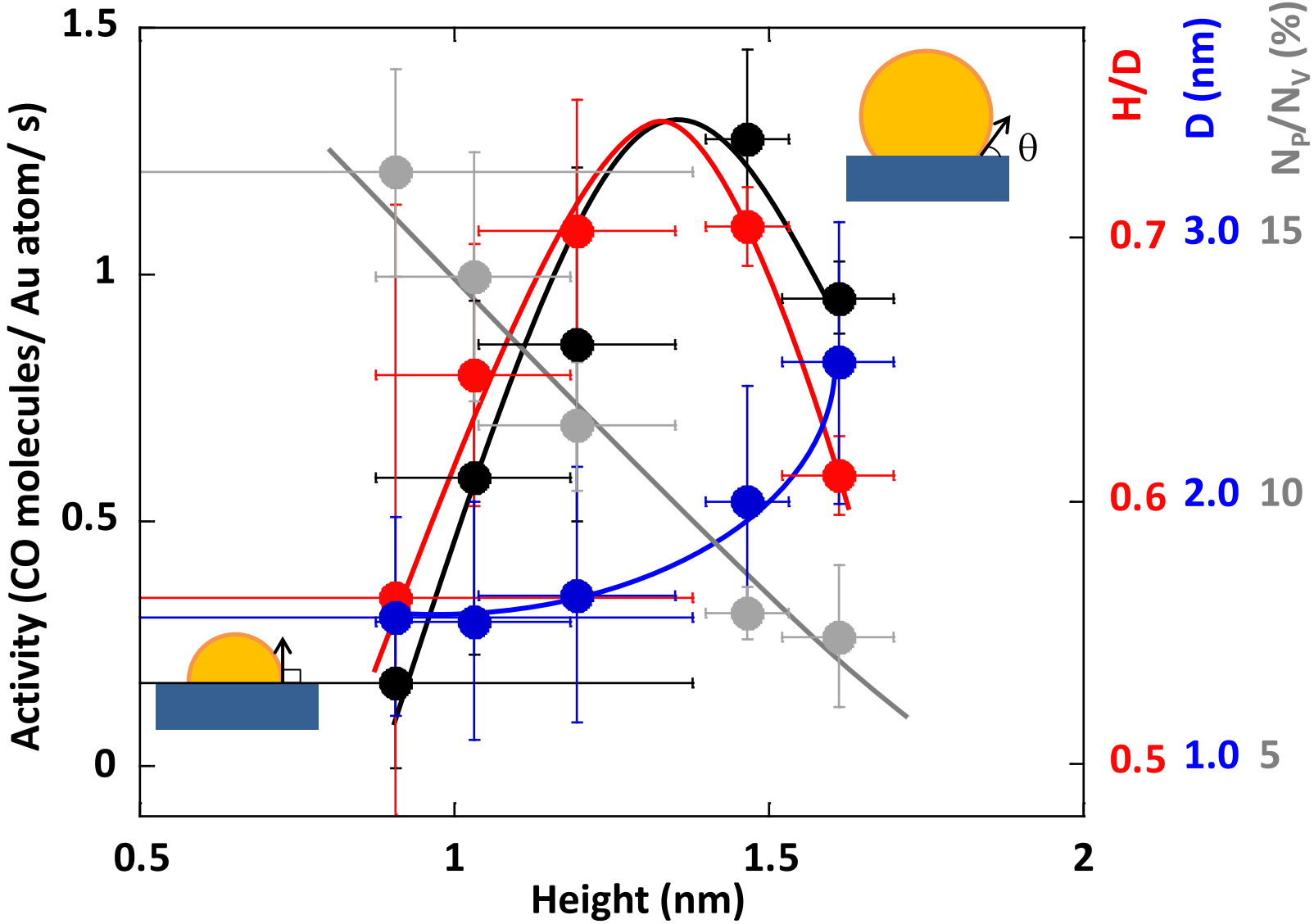
1.5
1
0.5
0
0.5
1
1.5
2
Activity (CO molecules/ Au atom/ s)
Height (nm)
θ
H/D
D (nm)
N_P/N_V (%)
0.7 3.0 15
0.6 2.0 10
0.5 1.0 5

Figure 6

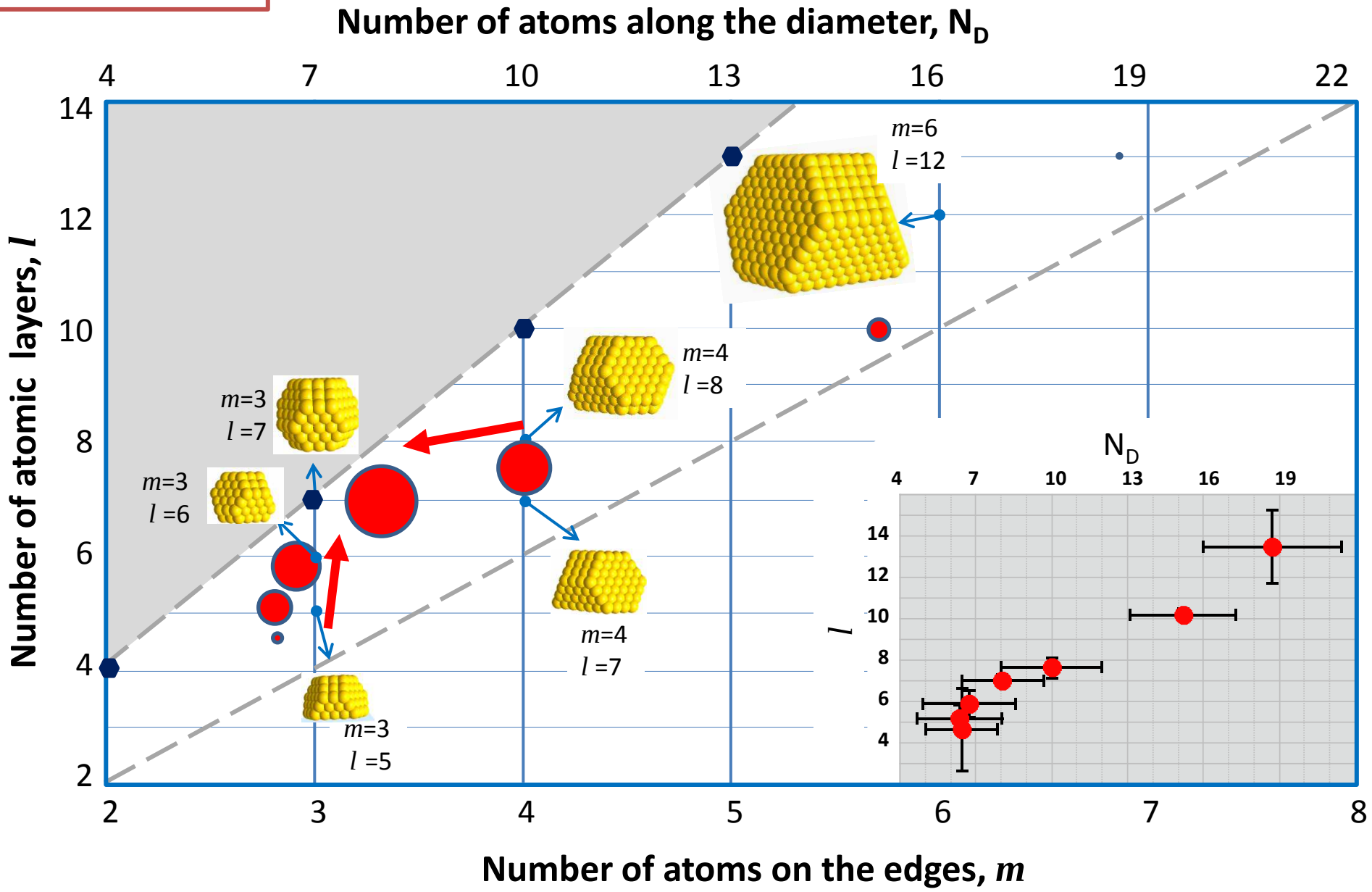
Number of atoms along the diameter, N_D
4
7
10
13
16
19
22
Number of atomic layers, l
14
12
10
8
6
4
2
2
3
4
5
6
7
8
Number of atoms on the edges, m
m=6
l =12
m=4
l =8
m=3
l =7
m=3
l =6
m=4
l =7
m=3
l =5
N_D
4
7
10
13
16
19
l
14
12
10
8
6
4